# Supplementary figures

## Sensitivity of clumped isotope temperatures in fossil benthic and planktic foraminifera to diagenetic alteration

Thomas J. Leutert[a]*, Philip F. Sexton[b], Aradhna Tripati[c,d], Alison Piasecki[a,e], Sze Ling Ho[a,f] and A. Nele Meckler[a]

[a]Bjerknes Centre for Climate Research and Department of Earth Science, University of Bergen, 5007 Bergen, Norway

[b]School of Environment, Earth & Ecosystem Sciences, The Open University, Milton Keynes MK7 6AA, UK

[c]Department of Earth, Planetary, and Space Sciences, Department of Atmospheric and Oceanic Sciences, Institute of the Environment and Sustainability, Center for Diverse Leadership in Science, University of California, Los Angeles, CA 90095, USA

[d]European Institute of Marine Sciences (IUEM), Université de Brest, UMR 6538, Domaines Océaniques, Rue Dumont D'Urville, and IFREMER, Laboratoire Géophysique et enregistrement Sédimentaire, 29280 Plouzané, France

[e]Department of Earth and Planetary Sciences, Harvard University, Cambridge, MA 02138, USA

[f]Institute of Oceanography, National Taiwan University, 10617 Taipei, Taiwan

Contents: 33 pages, 18 figures and captions

*Corresponding author:

E-mail: Thomas.Leutert@uib.no

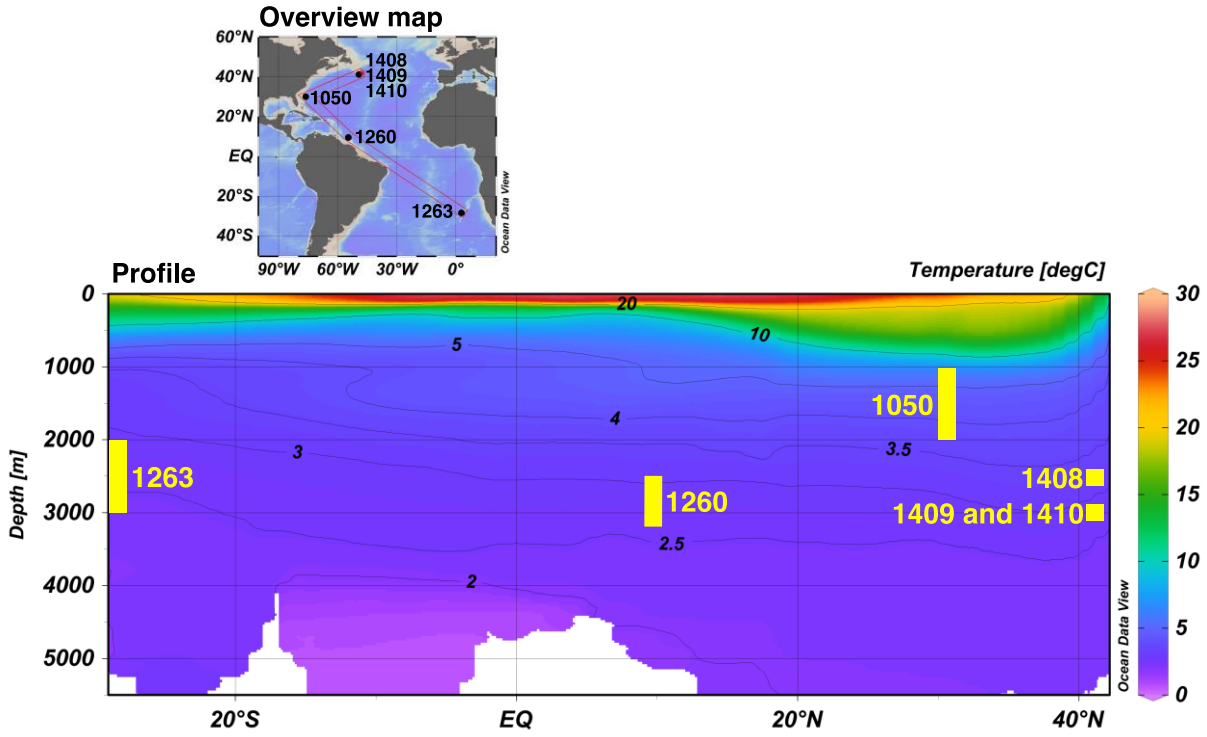


**Fig. S1:** Modern (1955-2012) mean annual temperature cross profile through all study sites. Estimated paleodepth ranges (Table 1) are marked in yellow. We analysed benthic foraminiferal material from Sites 1409, 1260 and 1263. At these sites, mean annual bottom water temperatures in the modern Atlantic Ocean range between around 2.5-3.5 °C, supporting our assumption of similar temperatures during benthic foraminiferal calcification. This figure was created using Ocean Data View (ODV) with temperature data from the World Ocean Atlas 2013 (Locarnini et al., 2013).

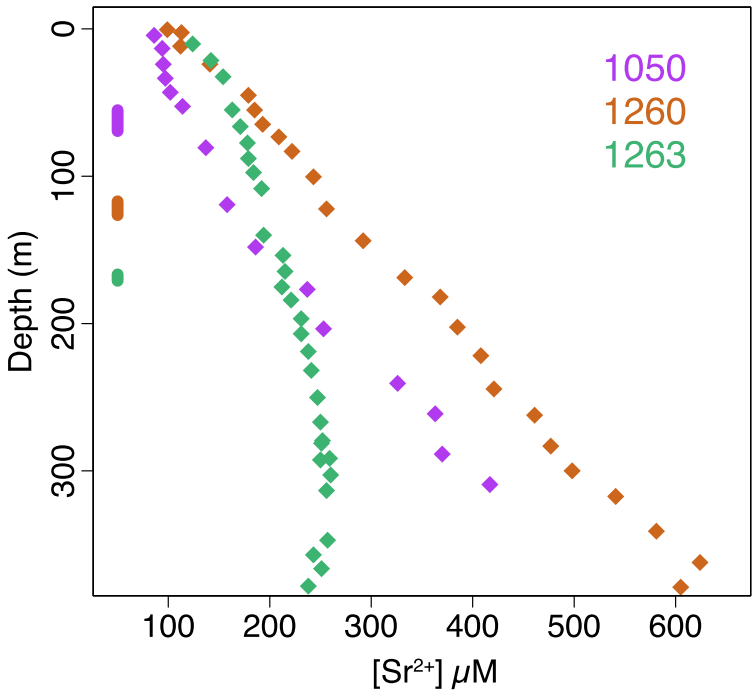


**Fig. S2:** Comparison of pore fluid $Sr^{2+}$ profiles at Sites 1050 (Norris et al., 1998), 1260 (Erbacher et al., 2004) and 1263 (Zachos et al., 2004). At Sites 1408, 1409 and 1410, pore fluid $Sr^{2+}$ concentrations were not measured. Pore fluid $Sr^{2+}$ is traditionally used as an indicator of diagenetic alteration, as dissolution and reprecipitation processes expel strontium in the coexisting pore fluids (e.g., Baker et al., 1982; Schrag et al., 1995). Sites 1050, 1260 and 1263 all show increases in pore fluid [$Sr^{2+}$] with depth in the sampling intervals. The observed increases with depth may be symptomatic for ongoing diagenetic alteration. However, this interpretation of $Sr^{2+}$ profiles in terms of diagenetic alteration is complicated by upward $Sr^{2+}$ diffusion from the basement, making it difficult to draw firm conclusions about the extent of diagenetic alteration of foraminiferal calcites (e.g., Edgar et al., 2013). Sample depth ranges at Sites 1050, 1260 and 1263 are shown by vertical lines. Our stable isotopic compositions as well as pore fluid $Sr^{2+}$ values from Site 1050 were measured on the

sediments of Hole A. Therefore, pore fluid $Sr^{2+}$ values are plotted against Hole A depth (Norris et al., 1998), whereas the pore fluid $Sr^{2+}$ values at Sites 1260 and 1263 are plotted against the respective shipboard composite depths (Erbacher et al., 2004; Zachos et al., 2004).

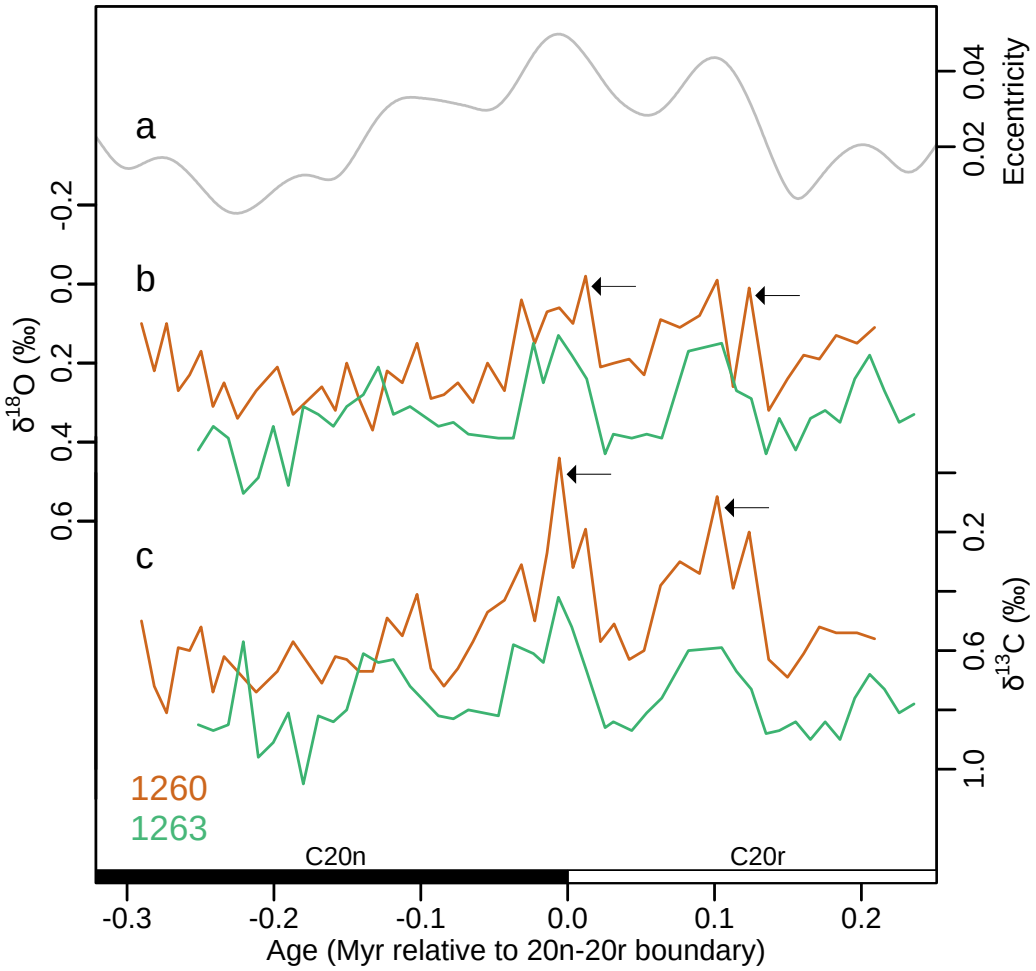


**Fig. S3:** (a) Eccentricity of orbital solution La2010d (Laskar et al., 2011) as well as benthic foraminiferal (b) $\delta^{18}O$ and (c) $\delta^{13}C$. In case of Site 1260, the semitransparent curves represent the age model of Westerhold and Röhl (2013), whereas the nontransparent curves the age model of this study. The agreement in both $\delta^{18}O$ and $\delta^{13}C$ between Site 1260 and 1263 as well as between Site 1260 and eccentricity is significantly improved by shifting the Site 1260-age model of Westerhold and Röhl (2013) 40 kyr forward in time. Lines are based on one measurement at each depth.

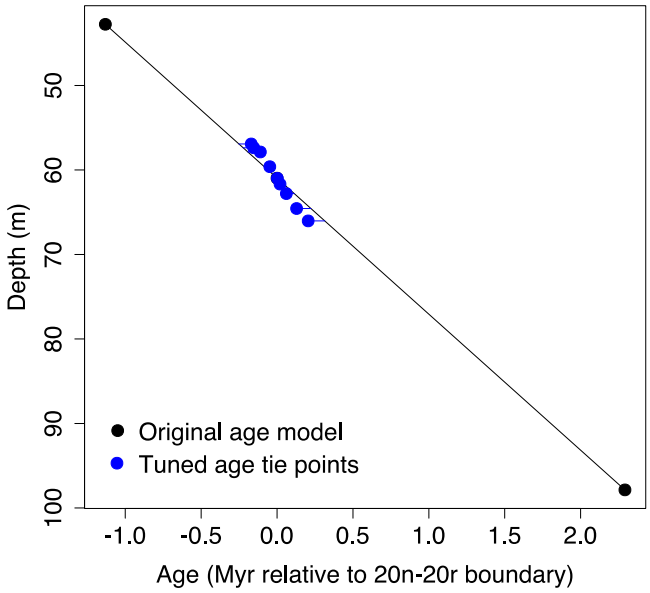


**Fig. S4:** Tuned age points used for linear interpolation at Site 1409 (blue) in comparison to the magnetochron boundary-based age model using GTS2012 (black) (Ogg, 2012; Vandenberghe et al., 2012). $\delta^{13}C$ increases and decreases at Site 1409 were tuned to those at Site 1263, using the software AnalySeries 2.0 (Paillard et al., 1996). Tuning depths can be found in Table S1.

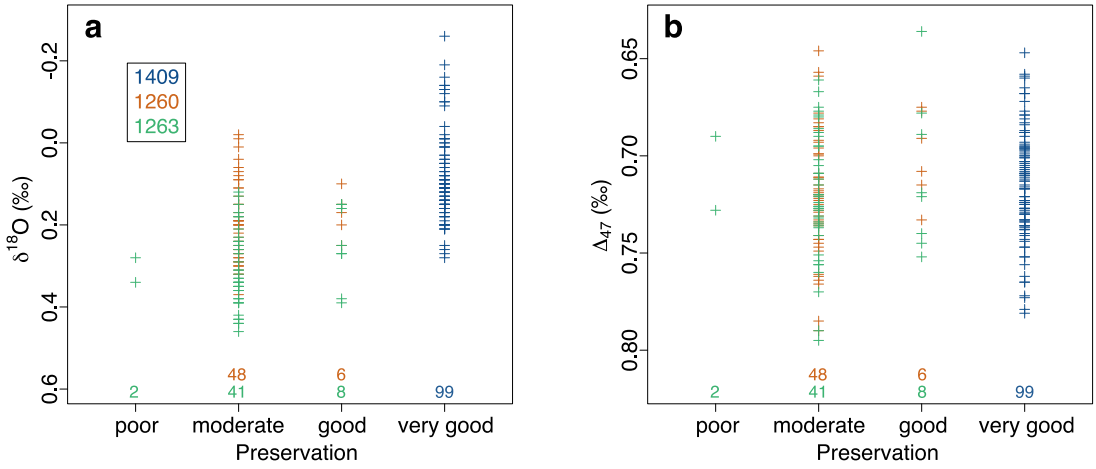


**Preservation classes for benthic foraminifera**

**poor**: moderate to extensive recrystallization visible, abundant overgrowth of large inorganic calcite crystals and/or signs of major dissolution

**moderate**: no to minor recrystallization, increased inorganic calcite overgrowth and/or signs of dissolution

**good**: no visible recrystallization, limited inorganic calcite overgrowth and/or dissolution

**very good**: no visible recrystallization, very limited amount of inorganic calcite overgrowth, no to very minor effects of dissolution visible

**Fig. S5:** Benthic $\delta^{18}O$ (a) and $\Delta_{47}$ (b) values of poorly, moderately, well and very well preserved foraminiferal tests. We rely on these qualitative classification classes in the current absence of a tool to quantify the amount of diagenetic calcite in a foraminiferal test. For each site, the number of observations per preservation class are listed at the bottom of the plots. Benthic foraminifera were first roughly classified under the light microscope based on test surface texture (preservation of microscale features such as pores), degree of translucence and test fragmentation. Then, a number of representative specimens from each site were further examined under the SEM to confirm and visualize potential dissolution, inorganic calcite overgrowths and recrystallization, and make the final classification. Note that we did the classification

in categories based on overall preservation of *N. truempyi* tests in each sample, although every sample typically includes a range of preservation states. SEM images documenting benthic foraminiferal preservation ranges at Sites 1409, 1260 and 1263 (including examples of poorly, moderately, well and very well preserved surface textures) are shown in Fig S6.

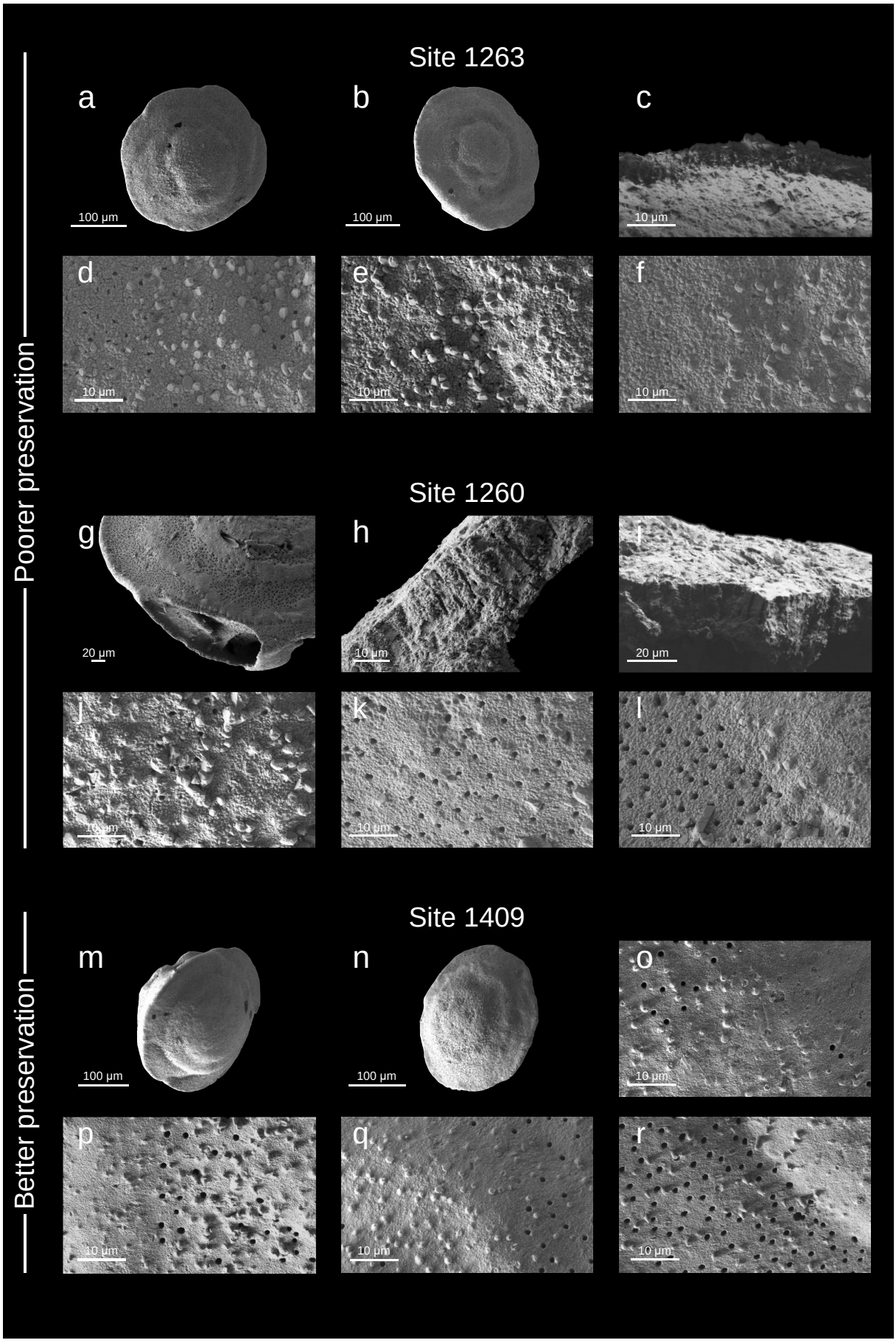
Site 1263
a
100 µm
b
100 µm
c
10 µm
d
10 µm
e
10 µm
f
10 µm
Site 1260
g
20 µm
h
10 µm
i
20 µm
j
10 µm
k
10 µm
l
10 µm
Site 1409
m
100 µm
n
100 µm
o
10 µm
p
10 µm
q
10 µm
r
10 µm
Poorer preservation
Better preservation

**Fig. S6:** Additional SEM images illustrating preservation states and preservation ranges of benthic foraminifera *N. truempyi* at Sites 1263 (a-f), 1260 (g-l) and 1409 (m-r). For each site, a number of different representative specimens are shown. As an example, the benthic foraminiferal wall texture shown in (e) appears poorly preserved. Here, pores are largely obscured by abundant overgrowths of inorganic calcite crystals. In comparison to (e), inorganic calcite crystals on the moderately preserved specimen shown in (d) are slightly smaller, overgrowths less extensive and pores mostly visible. The comparably well preserved wall texture shown in (k) is characterized by limited inorganic calcite overgrowth with only small crystallites. The very well preserved texture shown in (r) appears smooth without visible crystal faces or pore etching. The foraminifera were picked from samples 208-1263B-11H-4,91-93 (a-f), 207-1260B-10R-6,94-96 (g-l) and 342-U1409C-7H-4,110-112 (m-r).

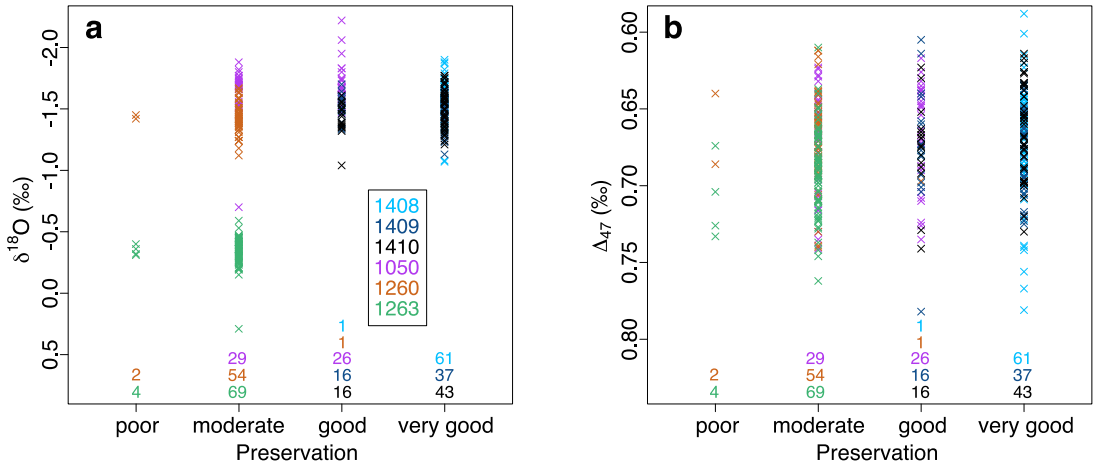


**Preservation classes for planktic foraminifera**

**poor**: extensive recrystallization, ubiquitous and massive inorganic calcite overgrowths and/or signs of major dissolution

**moderate**: some recrystallization, small inorganic calcite overgrowths and/or signs of dissolution

**good**: no visible recrystallization, signs of minor inorganic calcite overgrowths and/or minimal dissolution

**very good**: no visible recrystallization, no to very minor signs of inorganic calcite overgrowths, no effects of dissolution visible

**Fig. S7:** Planktic $\delta^{18}O$ (a) and $\Delta_{47}$ (b) values of poorly, moderately, well and very well preserved foraminiferal tests. For each site, the number of measurement values per preservation class are listed at the bottom of the plots. Similar to the classification of benthic foraminiferal preservation, the classification of planktic foraminiferal preservation states was done based on light microscopy in combination with SEM images of selected representative planktic foraminiferal tests. Note that planktic and benthic foraminiferal preservation classes are not identical. SEM images documenting planktic foraminiferal preservation ranges at each site are shown in Figs. S8 and S9. These figures include examples of poorly, moderately, well and very well preserved surface textures.

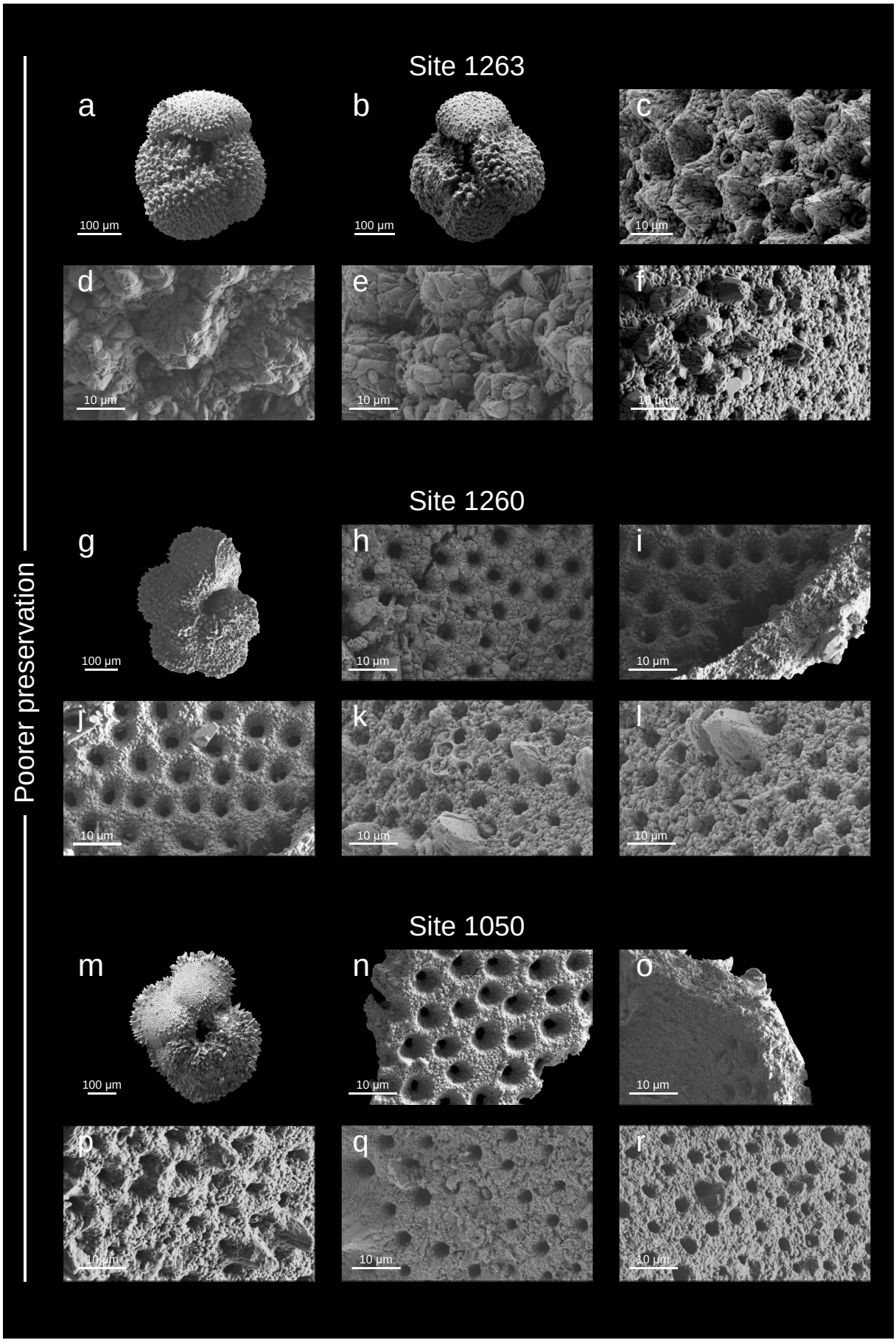
Site 1263
a
100 µm
b
100 µm
c
10 µm
d
10 µm
e
10 µm
f
10 µm
Site 1260
g
100 µm
h
10 µm
i
10 µm
j
10 µm
k
10 µm
l
10 µm
Site 1050
m
100 µm
n
10 µm
o
10 µm
p
10 µm
q
10 µm
r
10 µm
Poorer preservation

**Fig. S8:** Additional SEM images illustrating preservation states and preservation ranges of planktic foraminifera *A. bullbrooki* and *M. coronatus* at Sites 1263 (a-f), 1260 (g-l) and 1050 (m-r). For each site, a number of different representative specimens are shown. (d) and (e) display examples of poorly preserved planktic foraminiferal wall textures with ubiquitous overgrowths of massive calcite crystals, whereas calcite crystals covering the moderately preserved primary textures shown in (f) and (l) are smaller. Examples of well and very well preserved wall textures are presented in Fig. S9. The foraminifera were picked from samples 208-1263B-11H-6,51-53 (a, c, f), 208-1263B-11H-3,106-108 (b, d, e), 207-1260A-14R-5,146-148 (g-l), 171B-1050A-7H-5,102-104 (m, q, r) and 171B-1050A-7H-6,11-13 (n, o, p).

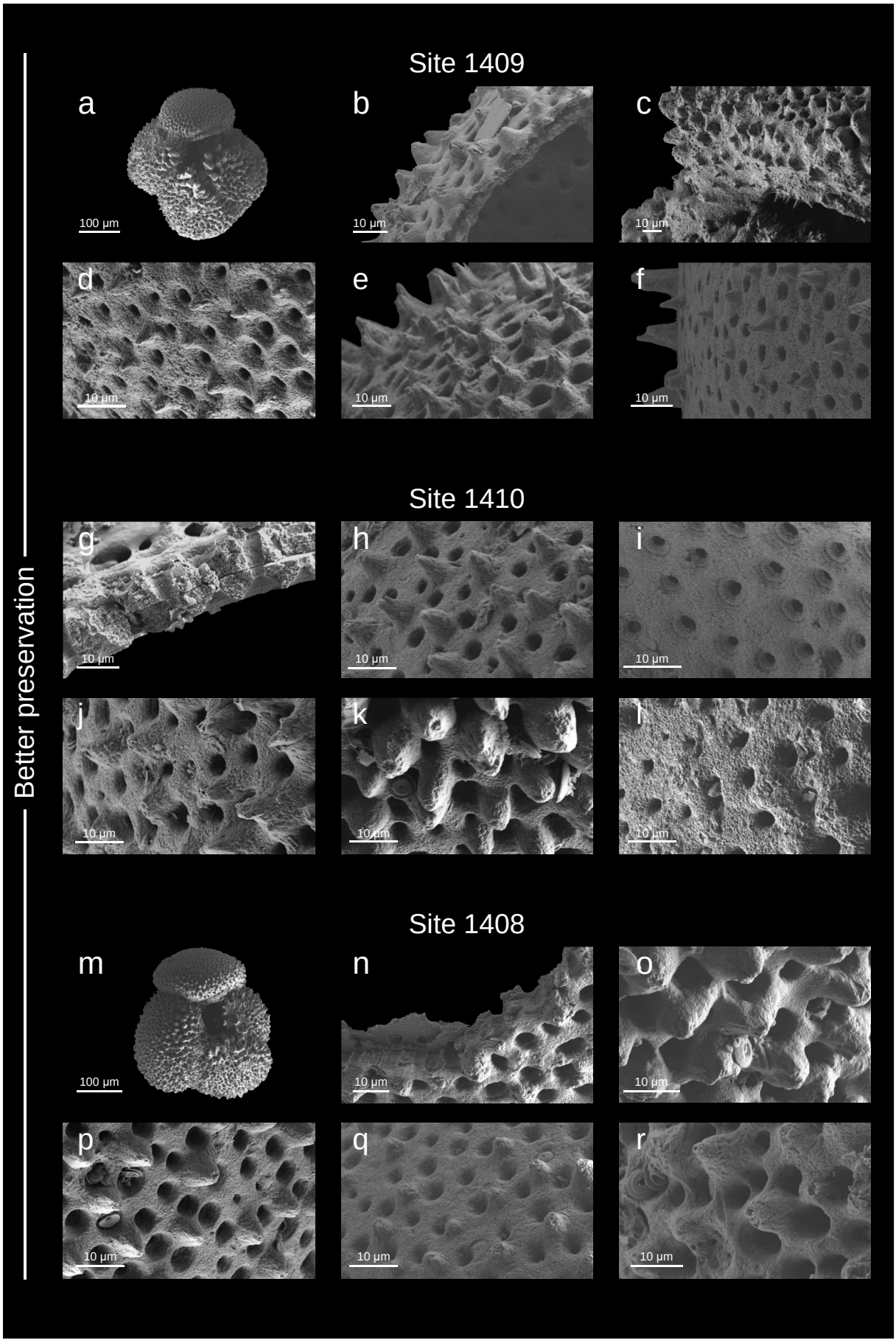
Site 1409
a
100 µm
b
10 µm
c
10 µm
d
10 µm
e
10 µm
f
10 µm
Site 1410
g
10 µm
h
10 µm
i
10 µm
j
10 µm
k
10 µm
l
10 µm
Site 1408
m
100 µm
n
10 µm
o
10 µm
p
10 µm
q
10 µm
r
10 µm
Better preservation

**Fig. S9:** Additional SEM images illustrating preservation states and preservation ranges of planktic foraminifera *A. bullbrooki* at Sites 1409 (a-f), 1410 (g-l) and 1408 (m-r). For each site, a number of different representative specimens are shown. Examples of well preserved wall textures are illustrated in (d) and (l). These wall textures appear slightly uneven (e.g., caused by dissolution) but exhibit only very small, hardly identifiable inorganic calcite crystals. For comparison, (o) and (p) show examples of very good preservation with purely biogenic surfaces and no visible signs of post-depositional alteration. The foraminifera were picked from samples 342-U1409C-7H-2,136-138 (a, c, d), 342-U1409C-7H-2,123-125 (b, e, f), 342-U1410C-17X-4,46-48 (g, h), 342-U1410C-17X-3,147-149 (i, j, k), 342-U1410C-17X-3,73-75 (l), 342-U1408C-17H-3,37-39 (m, n, o, q, r) and 342-U1408B-18H-2,109-111 (p).

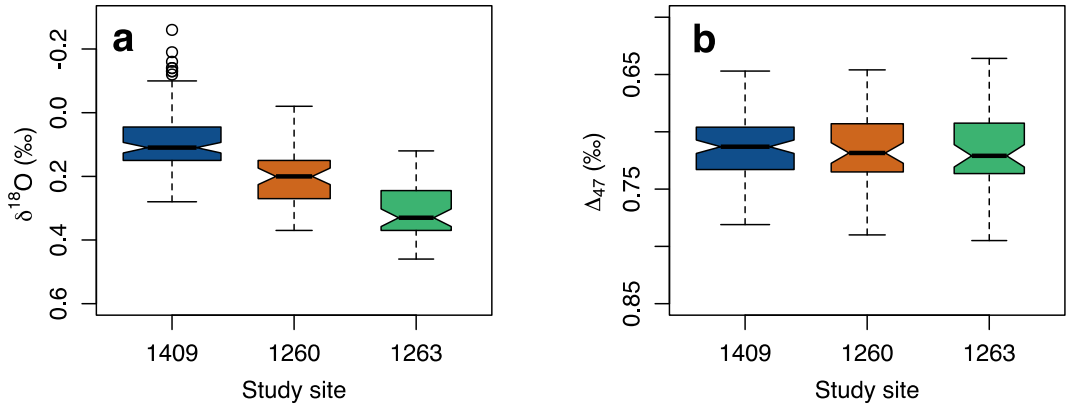


**Fig. S10:** Boxplots for benthic $\delta^{18}O$ (a) and $\Delta_{47}$ (b) values from -0.17 Myr to +0.21 Myr around the 20n/20r boundary. Boxes indicate lower and upper quartiles. Bold horizontal lines represent the median, whereas the lines extending vertically from the boxes (whiskers) illustrate the value ranges excluding outliers (circles). The boxplots were created using R with standard settings. Colors as defined in Fig. 1.

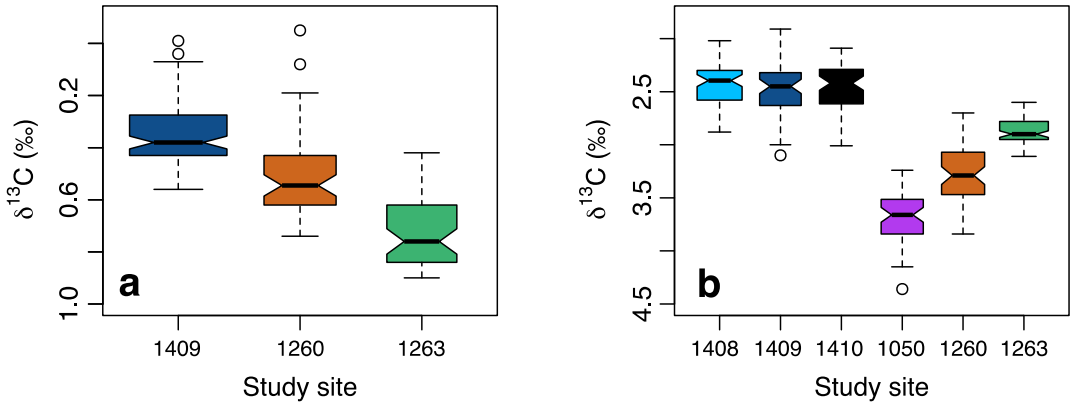


**Fig. S11:** Boxplots for benthic (a) and planktic (b) $\delta^{13}C$ values. Benthic and planktic data cover -0.17 Myr to +0.21 Myr and -0.15 Myr to +0.21 Myr around the 20n/20r boundary, respectively. The boxplots were created using R with standard settings. Colors as defined in Fig. 1.

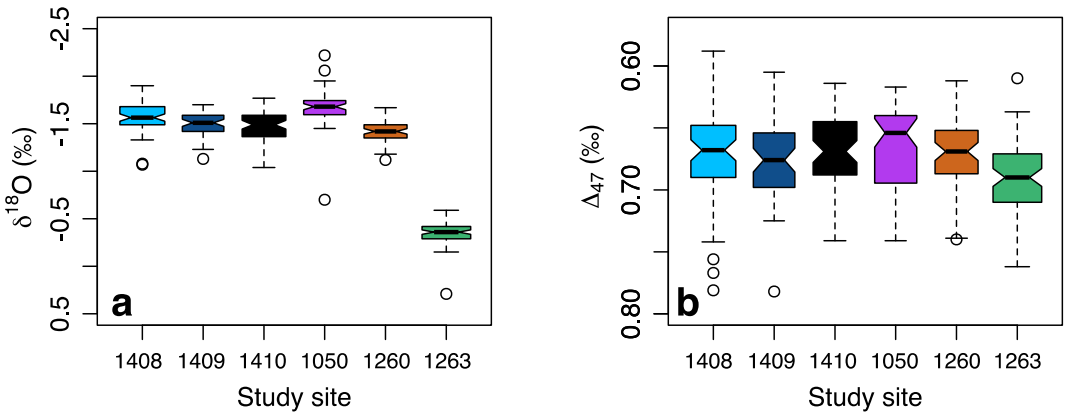


**Fig. S12:** Boxplots for planktic $\delta^{18}O$ (a) and $\Delta_{47}$ (b) covering -0.15 Myr to +0.21 Myr around the 20n/20r boundary. The boxplots were created using R with standard settings. Colors as defined in Fig. 1.

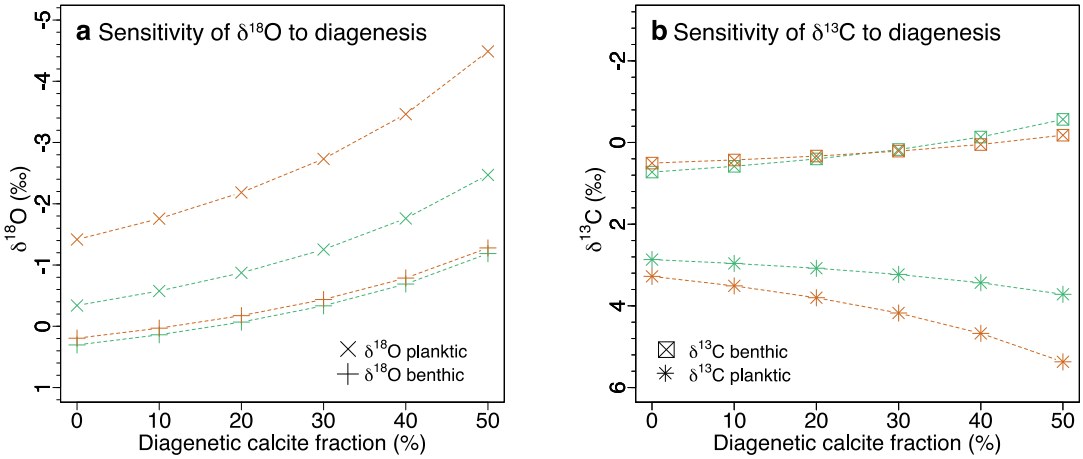


**Fig. S13:** Sensitivities of foraminiferal $\delta^{18}O$ and $\delta^{13}C$ values to diagenesis. Initial biogenic $\delta^{18}O$ (a) and $\delta^{13}C$ (b) signatures were modeled for different fractions of inorganic calcite. For this modeling, we utilized the $^{18}O$ fractionation factor of Watkins et al. (2013). Similar to $\delta^{18}O$, planktic $\delta^{13}C$ seems to be more susceptible to diagenetic alteration than benthic $\delta^{13}C$. Colors as defined in Fig. 1.

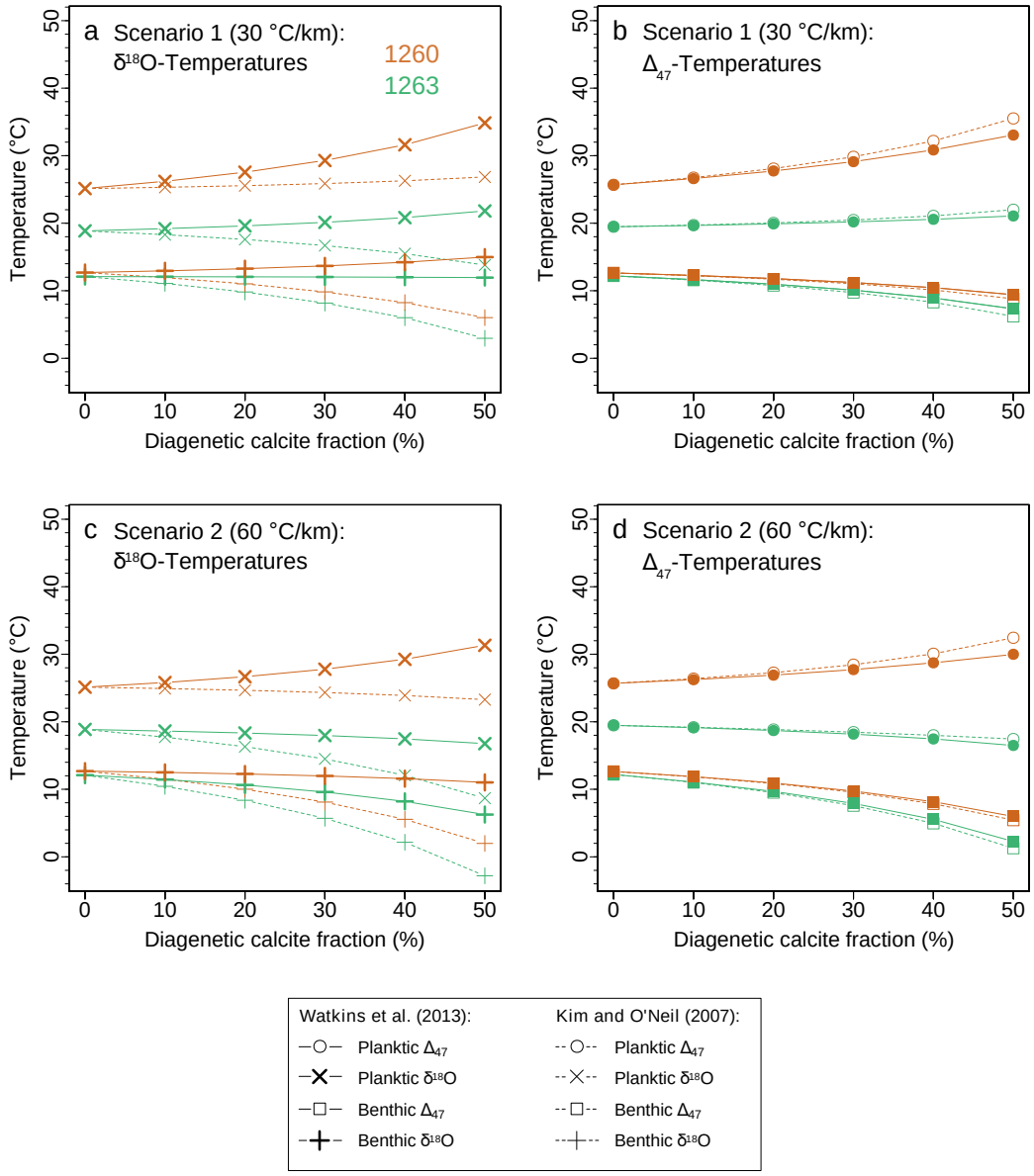


**Fig. S14:** Effects of late diagenesis near final sediment burial depths on modeled biogenic calcification temperatures ($\delta^{18}O$ and $\Delta_{47}$). Similar to Sexton et al. (2006), two different geothermal gradient estimates were used to approach the geothermal gradient during the middle Eocene and define two scenarios of late (deep) diagenesis: (1) 30 °C/km (a, b) and (2) 60 °C/km (c, d) (Zwart et al., 1996; Rao et al., 2001; Stolper et al., 2018). In addition, we utilized a pore fluid $\delta^{18}O$ gradient of -2.5

‰/km (Lawrence and Gieskes, 1981; Sexton and Wilson, 2009) and our site-specific clumped isotope DSTs averaged over the relevant interval (temperatures at 0 m below sea floor) to calculate pore fluid $\delta^{18}O$ and temperatures at final sediment burial depths in both scenarios of deep diagenesis. Constant gradients in pore fluid $\delta^{18}O$ and temperature were assumed, due to a lack of better constraint for Sites 1260 and 1263 during the middle Eocene. For the same reason, pore fluid $\delta^{13}O$ gradients in these high carbonate, low organic matter sediments were assumed to be 0 ‰/km. Sediments from Site 1260 were taken from around 117 m to 129 m burial depth and sediments from Site 1263 were taken from around 170 m to 174 m burial depth (Table 1). In both scenarios, deep diagenesis at Sites 1260 and 1263 is assumed to occur in depths of 117 m and 170 m, respectively (approximate locations of uppermost samples at each site). For the modeling of DSTs at Site 1260, calculated temperatures of diagenetic calcite precipitation are 16.1 °C and 19.7 °C in Scenarios 1 and 2, respectively. Furthermore, diagenetic calcite $\delta^{18}O$ compositions in Scenarios 1 and 2 are 0.62 ‰ and -0.12 ‰, respectively, when assuming the $^{18}O$ fractionation factor of Watkins et al. (2013), and -1.04 ‰ and -1.79 ‰, respectively, when assuming the $^{18}O$ fractionation factor of Kim and O'Neil (1997). At Site 1263, diagenetic calcite precipitation temperatures are 17.3 °C and 22.4 °C in Scenarios 1 and 2, whereas diagenetic calcite $\delta^{18}O$ compositions are 0.28 ‰ and -0.78 ‰ for $^{18}O$ fractionation according to Watkins et al. (2013), and -1.39 ‰ and -2.46 ‰ for $^{18}O$ fractionation according to Kim and O'Neil (1997). Similar to the scenario of early burial diagenesis described in Table 2, inorganic calcite precipitation temperature and $\delta^{18}O$ values used for SST modeling are very similar to the values used for DST modeling, and thus not listed explicitly. Deep and shallow diagenesis values are compared in Fig. S15.

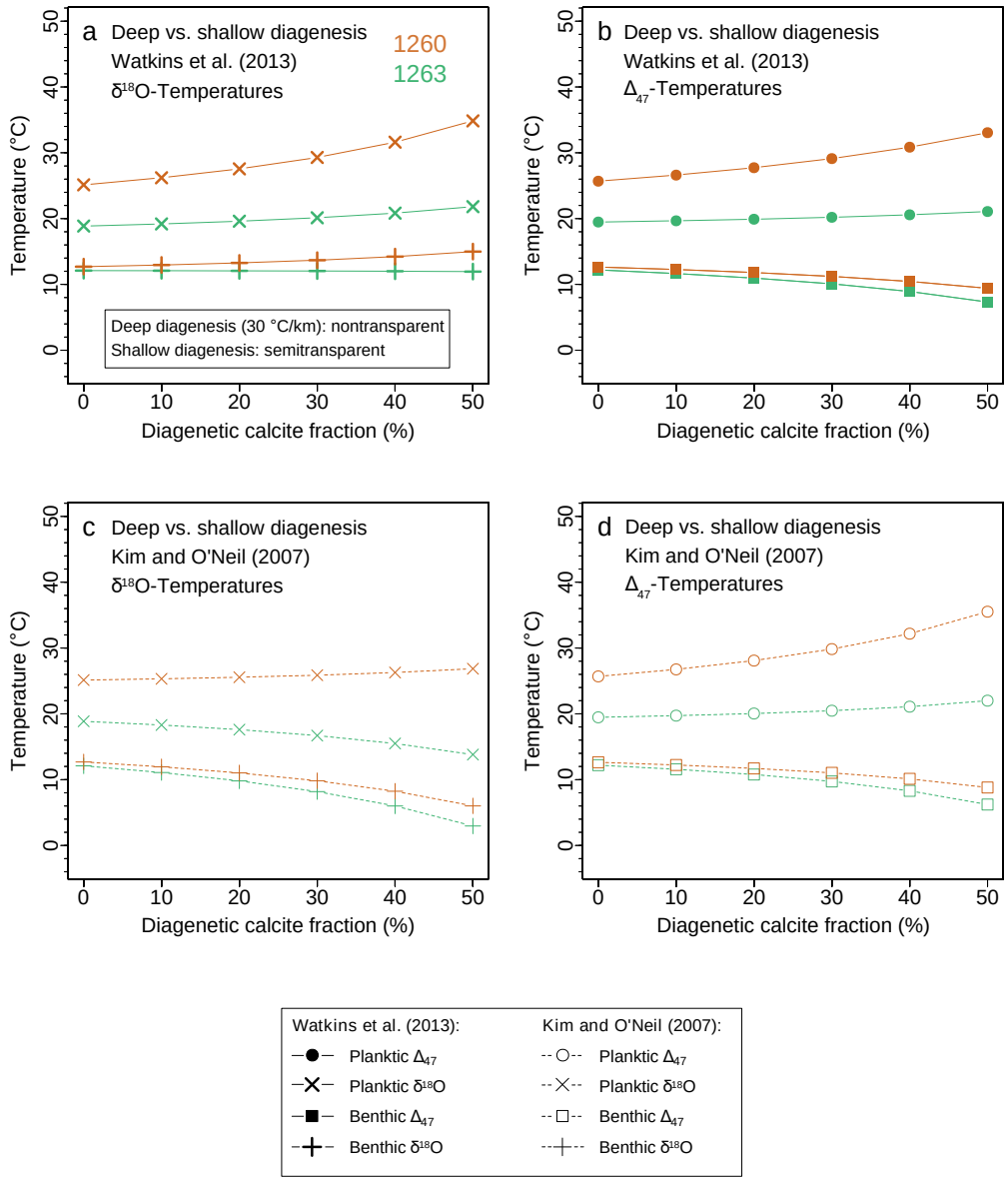


**Fig. S15:** Comparison of deep (nontransparent) and shallow (semitransparent) diagenetic effects on modeled biogenic calcification temperatures ($\delta^{18}O$ and $\Delta_{47}$). $\delta^{18}O$-based temperature values are shown in (a) and (c), whereas $\Delta_{47}$-based temperatures are shown in (b) and (d). The deep diagenesis values are identical to the values shown in Figs. S14a and S14b (geothermal gradient of 30 °C/km), whereas the shallow diagenesis values are identical to the values shown in Fig. 8. In

comparison to shallow diagenesis, deeper diagenesis would imply a smaller cool bias in SSTs reconstructed from the $\delta^{18}O$- and $\Delta_{47}$-signatures of planktic foraminiferal tests and benthic foraminiferal DSTs that are potentially too high.

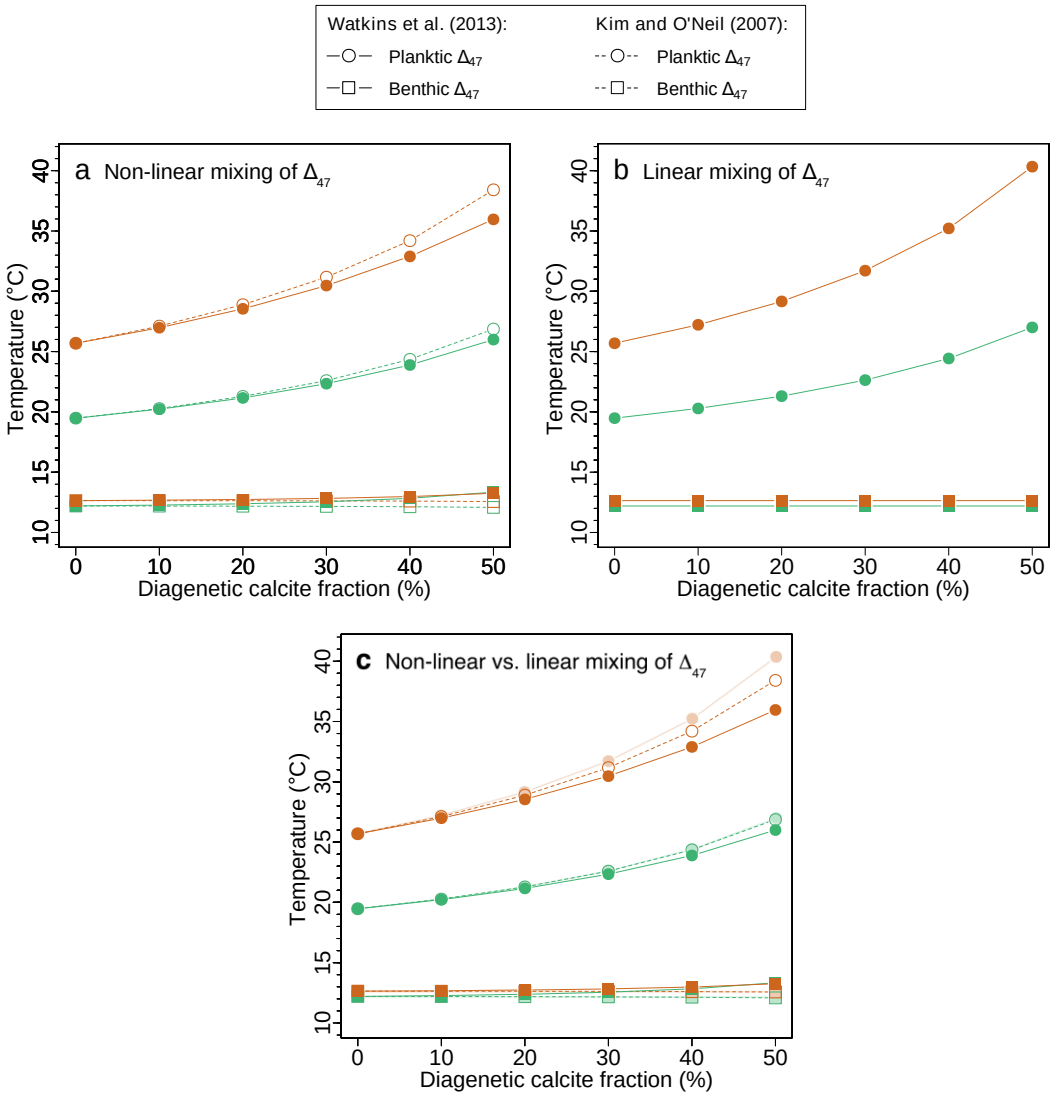


**Fig. S16:** Effects of non-linear mixing on modeled $\Delta_{47}$-based temperatures. Temperatures of initial biogenic calcification are plotted for (a) non-linear and (b) linear $\Delta_{47}$ mixing. Panel (c) shows non-linear (nontransparent) vs. linear (semitransparent) mixing of $\Delta_{47}$. (a) is identical to Fig. 8b. We used the $^{18}O$ fractionation factors of Watkins et al. (2013) (filled circles) and Kim and O'Neil (1997) (open circles) for our non-linear mixing calculations. The curves in (b) visualizing linear mixing have been calculated based on the assumption that the $\Delta_{47}$ values of frosty foraminiferal tests represent weighted averages (linear mixing) of the $\Delta_{47}$

values of glassy biogenic calcite and inorganic calcite formed during post-depositional diagenesis. Therefore, these values are independent of the $^{18}O$ fractionation factor. The comparison of non-linear and linear mixing of $\Delta_{47}$ (c) shows a reduced susceptibility of planktic foraminiferal $\Delta_{47}$ to diagenesis when considering non-linear mixing effects. Colors as defined in Fig. 1.

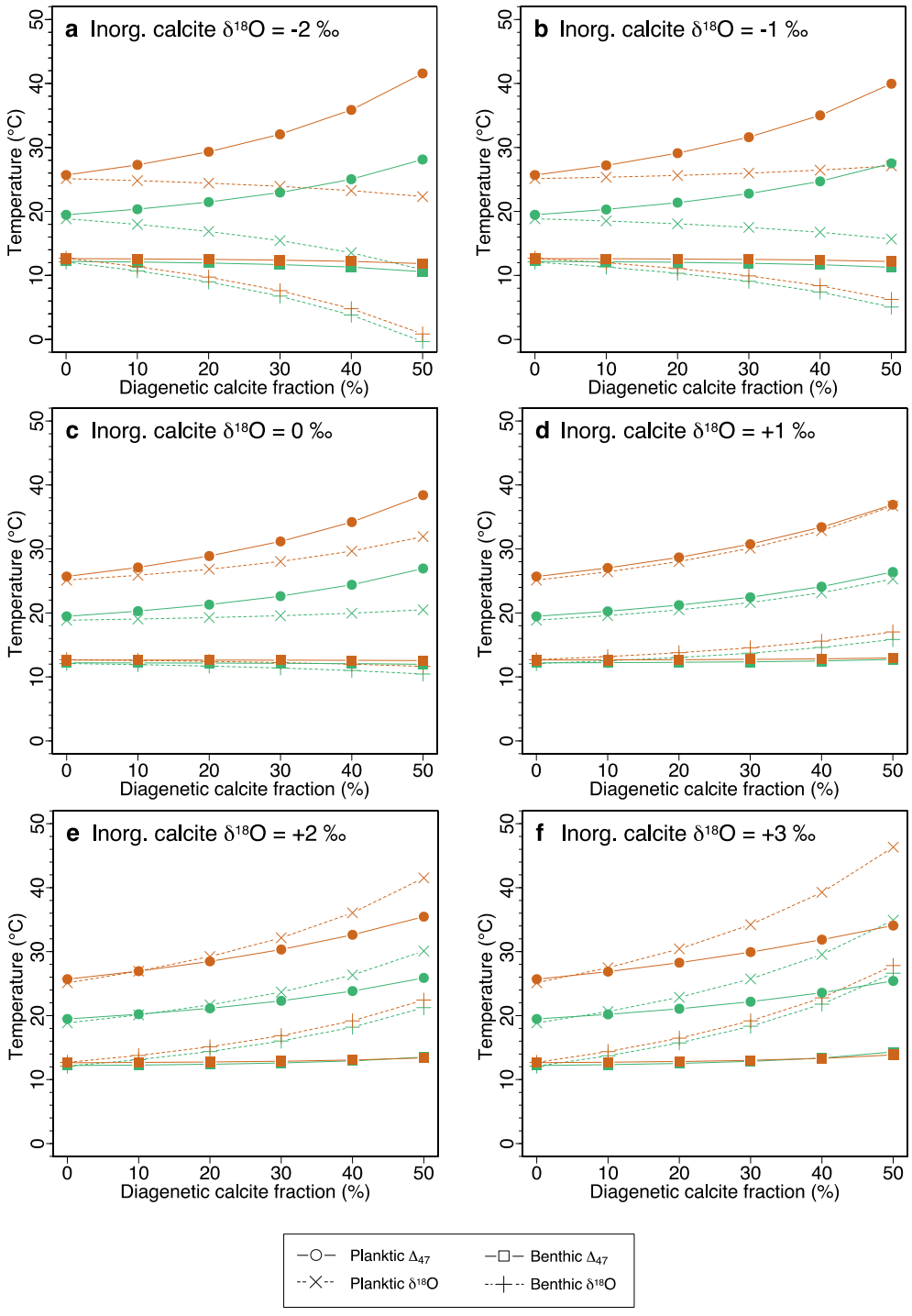


**Fig. S17:** Sensitivity of modeled biogenic calcification temperatures ($\delta^{18}O$ and $\Delta_{47}$) to different inorganic $\delta^{18}O$ compositions. $\delta^{18}O$ values of pore fluids and inorganic calcite precipitated during early diagenesis may be influenced by local effects and thus

difficult to estimate without direct measurements. Therefore, inorganic calcite $\delta^{18}O$ values of (a) -2 ‰, (b) -1 ‰, (c) 0 ‰, (d) +1 ‰, (e) +2 ‰ and (f) +3 ‰, spanning the range of published values (e.g., Pearson et al., 2001; Tripati et al., 2003; Kozdon et al., 2013; Voigt et al., 2016), were used to test the effect of inorganic calcite $\delta^{18}O$ on diagenetic alteration. Temperature values are based on planktic (crosses) and benthic (plus signs) foraminiferal $\delta^{18}O$ as well as on planktic (circles) and benthic (squares) foraminiferal $\Delta_{47}$. For this sensitivity test, the $^{18}O$ fractionation factor does not matter, as inorganic calcite $\delta^{18}O$ is prescribed. Colors as defined in Fig. 1.

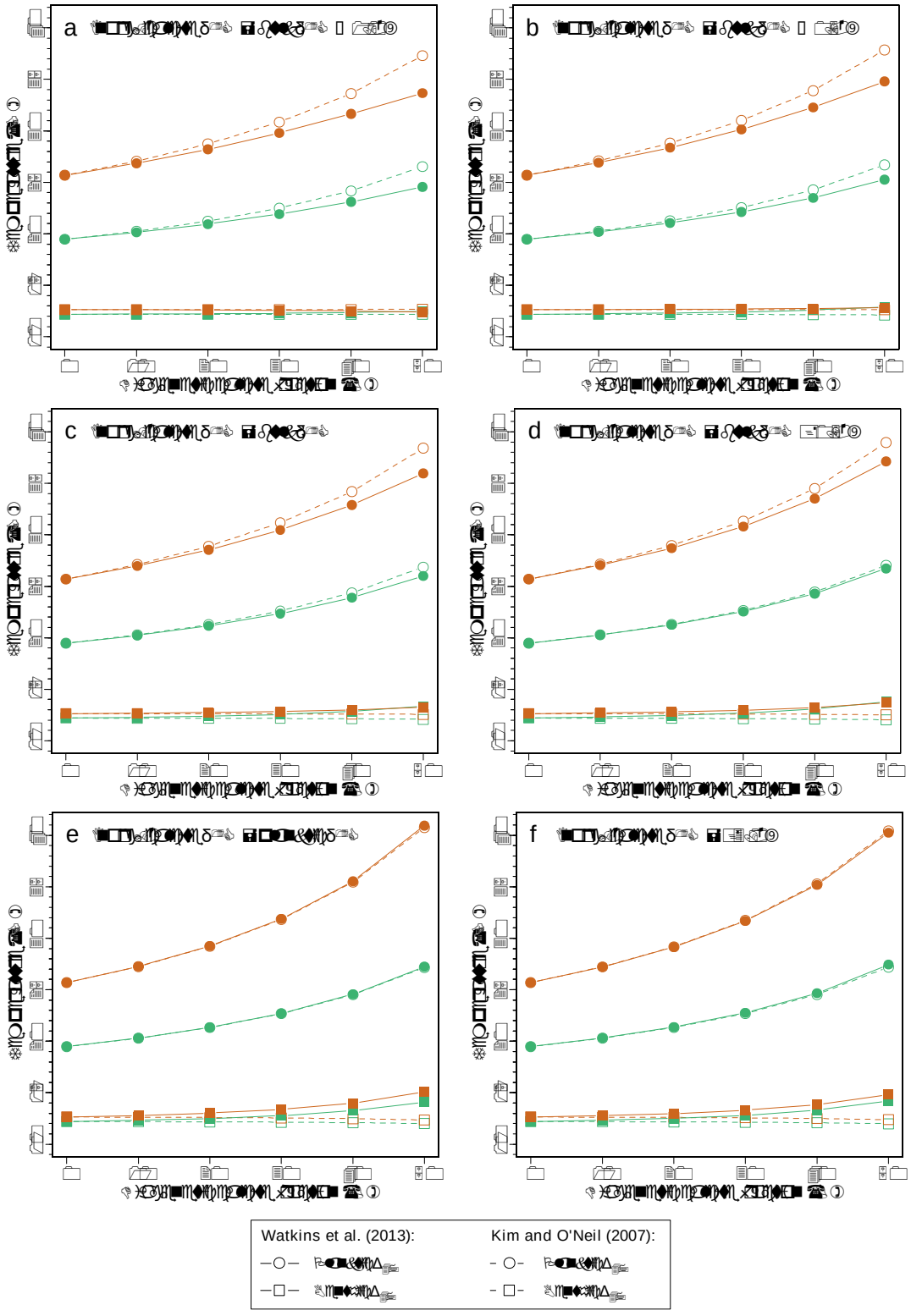


**Fig. S18:** Sensitivity of modeled biogenic calcification temperatures ($\Delta_{47}$) to different inorganic $\delta^{13}C$ compositions. The approximation of inorganic calcite $\delta^{13}C$ by bulk

$\delta^{13}C$ (Table 2) may be complicated by local effects. Furthermore, bulk $\delta^{13}C$ values for Site 1260 (Edgar et al., 2007) were taken from a slightly different time interval during the middle Eocene (roughly 42 Ma). Using the $^{18}O$ fractionation factors of Watkins et al. (2013) (filled circles) and Kim and O'Neil (1997) (open circles), we performed a sensitivity study to test the effect of different assumptions for inorganic calcite $\delta^{13}C$ on the susceptibility of clumped isotope temperatures to diagenesis. For that, we assumed inorganic calcite $\delta^{13}C$ values that are (a) 1.0 ‰ lower than bulk $\delta^{13}C$, (b) 0.5 ‰ lower than bulk $\delta^{13}C$ and (d) 0.5 ‰ higher than bulk $\delta^{13}C$. In addition, we used (e) site-specific planktic $\delta^{13}C$ averaged over the overlapping time interval to approximate inorganic calcite $\delta^{13}C$ as well as (f) absolute inorganic calcite $\delta^{13}C$ equals 3.0 ‰, similar to Pearson et al. (2001). (c) is identical to Fig. 8b. Temperature values are based on planktic (circles) and benthic (squares) foraminiferal $\Delta_{47}$. Colors as defined in Fig. 1.

References

Baker, P.A., Gieskes, J.M. and Elderfield, H. (1982) Diagenesis of Carbonates in Deep-Sea Sediments - Evidence from Sr/Ca Ratios and Interstitial Dissolved $Sr^{2+}$ Data. *Journal of Sedimentary Petrology* **52,** 71-82.

Edgar, K.M., Pälike, H. and Wilson, P.A. (2013) Testing the impact of diagenesis on the $\delta^{18}O$ and $\delta^{13}C$ of benthic foraminiferal calcite from a sediment burial depth transect in the equatorial Pacific. *Paleoceanography* **28,** 468-480.

Edgar, K.M., Wilson, P.A., Sexton, P.F. and Suganuma, Y. (2007) No extreme bipolar glaciation during the main Eocene calcite compensation shift. *Nature* **448,** 908-911.

Erbacher, J., Mosher, D.C., Malone, M.J. and the Expedition 207 Scientists (2004) Site 1260, *Proceedings of the Ocean Drilling Program, Initial Reports Volume 207*, pp. 1-113.

Kim, S.T. and O'Neil, J.R. (1997) Equilibrium and nonequilibrium oxygen isotope effects in synthetic carbonates. *Geochimica et Cosmochimica Acta* **61,** 3461-3475.

Kozdon, R., Kelly, D.C., Kitajima, K., Strickland, A., Fournelle, J.H. and Valley, J.W. (2013) In situ $\delta^{18}O$ and Mg/Ca analyses of diagenetic and planktic foraminiferal calcite preserved in a deep-sea record of the Paleocene-Eocene thermal maximum. *Paleoceanography* **28,** 517-528.

Laskar, J., Fienga, A., Gastineau, M. and Manche, H. (2011) La2010: a new orbital solution for the long-term motion of the Earth. *Astronomy & Astrophysics* **532**.

Lawrence, J.R. and Gieskes, J.M. (1981) Constraints on Water Transport and Alteration in the Oceanic Crust from the Isotopic Composition of Pore Water. *Journal of Geophysical Research* **86,** 7924-7934.

Locarnini, R.A., Mishonov, A.V., Antonov, J.I., Boyer, T.P., Garcia, H.E., Baranova, O.K., Zweng, M.M., Paver, C.R., Reagan, J.R., Johnson, D.R., Hamilton, M. and Seidov, D. (2013) World Ocean Atlas 2013, Volume 1: Temperature. S. Levitus, Ed., A. Mishonov Technical Ed. *NOAA Atlas NESDIS 73***,** 40.

Norris, R.D., Kroon, D., Klaus, A. and the Expedition 171B Scientists (1998) Site 1050, *Proceedings of the Ocean Drilling Program, Initial Reports, Vol. 171B*, pp. 93-169.

Ogg, J.G. (2012) Chapter 5 – Geomagnetic Polarity Time Scale, in: Gradstein, F.M., Ogg, J.G., Schmitz, M.D., and Ogg, G.M. (Eds.), *The Geologic Time Scale*. Elsevier, Boston, pp. 85-113.

Paillard, D., Labeyrie, L. and Yiou, P. (1996) Macintosh program performs time-series analysis. *Eos Trans. AGU* **77,** 379.

Pearson, P.N., Ditchfield, P.W., Singano, J., Harcourt-Brown, K.G., Nicholas, C.J., Olsson, R.K., Shackleton, N.J. and Hall, M.A. (2001) Warm tropical sea surface temperatures in the Late Cretaceous and Eocene epochs. *Nature* **414,** 481-487.

Rao, Y.H., Subrahmanyam, C., Sharma, S.R., Rastogi, A.A. and Deka, B. (2001) Estimates of geothermal gradients and heat flow from BSRs along the Western Continental Margin of india. *Geophysical Research Letters* **28,** 355-358.

Schrag, D.P., DePaolo, D.J. and Richter, F.M. (1995) Reconstructing Past Sea-Surface Temperatures - Correcting for Diagenesis of Bulk Marine Carbonate. *Geochimica et Cosmochimica Acta* **59,** 2265-2278.

Sexton, P.F. and Wilson, P.A. (2009) Preservation of benthic foraminifera and reliability of deep-sea temperature records: Importance of sedimentation rates, lithology, and the need to examine test wall structure. *Paleoceanography* **24**.

Sexton, P.F., Wilson, P.A. and Pearson, P.N. (2006) Microstructural and geochemical perspectives on planktic foraminiferal preservation: "Glassy" versus "Frosty". *Geochemistry Geophysics Geosystems* **7**.

Stolper, D.A., Eiler, J.M. and Higgins, J.A. (2018) Modeling the effects of diagenesis on carbonate clumped-isotope values in deep- and shallow-water settings. *Geochimica et Cosmochimica Acta* **227,** 264-291.

Tripati, A.K., Delaney, M.L., Zachos, J.C., Anderson, L.D., Kelly, D.C. and Elderfield, H. (2003) Tropical sea-surface temperature reconstruction for the early Paleogene using Mg/Ca ratios of planktonic foraminifera. *Paleoceanography* **18**.

Vandenberghe, N., Hilgen, F.J., Speijer, R.P., Ogg, J.G., Gradstein, F.M., Hammer, O., Hollis, C.J. and Hooker, J.J. (2012) Chapter 28 – The Paleogene Period, in: Gradstein, F.M., Ogg, J.G., Schmitz, M.D., and Ogg, G.M. (Eds.), *The Geologic Time Scale*. Elsevier, Boston, pp. 855-921.

Voigt, J., Hathorne, E.C., Frank, M. and Holbourn, A. (2016) Minimal influence of recrystallization on middle Miocene benthic foraminiferal stable isotope stratigraphy in the eastern equatorial Pacific. *Paleoceanography* **31,** 98-114.

Watkins, J.M., Nielsen, L.C., Ryerson, F.J. and DePaolo, D.J. (2013) The influence of kinetics on the oxygen isotope composition of calcium carbonate. *Earth and Planetary Science Letters* **375,** 349-360.

Westerhold, T. and Röhl, U. (2013) Orbital pacing of Eocene climate during the Middle Eocene Climate Optimum and the chron C19r event: Missing link found

in the tropical western Atlantic. *Geochemistry Geophysics Geosystems* **14,** 4811-4825.

Zachos, J.C., Kroon, D., Blum, P. and the Expedition 208 Scientists (2004) Site 1263, *Proceedings of the Ocean Drilling Program, Initial Reports Volume 208*, pp. 1-87.

Zwart, G., Moore, J.C. and Cochrane, G.R. (1996) Variations in temperature gradients identify active faults in the Oregon accretionary prism. *Earth and Planetary Science Letters* **139,** 485-495.